J Intell Robot Syst (2014) 74:147–172
DOI 10.1007/s10846-013-9960-1

Estimating Vehicle State by GPS/IMU Fusion with Vehicle Dynamics

Kamal Saadeddin · Mamoun F. Abdel-Hafez · Mohammad Amin Jarrah

Received: 22 July 2013 / Accepted: 14 September 2013 / Published online: 4 October 2013

Abstract In this paper, a low-cost navigation system with high integrity and reliability is proposed. A high-integrity estimation filter is proposed to obtain a high-accuracy state estimate. The filter utilizes a vehicle velocity constraint measurement to enhance the accuracy of the estimate. Two estimation filters, the extended Kalman filter (EKF) and the extended information filter (EIF), are designed and compared to obtain the estimate of the vehicle state. An instrumentation system that consists of a microcontroller, GPS receiver, IMU, velocity encoder, and Zigbee transceiver is used. The microcontroller provides a vehicle navigation solution at 50 Hz by fusing the measurements of the IMU and GPS receiver using the proposed filter design. Extensive experimental tests are conducted to verify the accuracy of the proposed algorithm. These results are processed with and without the velocity constraints. The estimation accuracy improvement with the addition of the velocity constraints is shown. A more than 16 % reduction in the computational time is demonstrated when using the EIF in comparison to the EKF approach.

Keywords GPS · IMU · State estimation · Velocity constraint

K. Saadeddin · M. F. Abdel-Hafez (✉) · M. A. Jarrah
Department of Mechanical Engineering,
American University of Sharjah, Sharjah, UAE
e-mail: mabdelhafez@aus.edu

K. Saadeddin
e-mail: b00024496@aus.edu

M. A. Jarrah
e-mail: mjarrah@aus.edu

1 Introduction

High-accuracy and low-cost estimation of vehicle state is vital for autonomous navigation and control applications. If the vehicle state is estimated accurately with low computational demand, then the vehicle can be guided along the desired trajectory. Also, if more than one vehicle is assigned a certain task, then the accurate knowledge of the vehicle's relative state will ensure the safe operation of the overall system.

In this paper, a navigation system that calculates the state of each vehicle at a 50-Hz rate is proposed. Using wireless transceivers such as Zigbee, this state is continuously transmitted to neighboring vehicles. In the proposed navigation system, a low-cost GPS receiver measures the position and velocity of the vehicle at a frequency of 5 Hz. Three-axis accelerometers and gyroscopes measure the linear acceleration and angular velocity of the vehicle at 50 Hz. Also, velocity encoders are used to measure the forward velocity of the vehicle. The velocity measurement can be obtained

from the airspeed measurement of an unmanned aircraft system (UAS) or from wheel encoders for ground vehicles.

Using measurements from the GPS receiver and the forward velocity constraint, the three-axis acceleration and angular velocity measurements are integrated to obtain the position and velocity of the vehicle at 50 Hz [1–5]. The position and velocity along with the identity code of the vehicle (ID) are then transmitted to neighboring vehicles using a Zigbee transceiver [6–8], see Fig. 1.

There have been a number of studies aimed at reducing vehicle accidents using different approaches and navigation algorithms. The use of encoders, GPS receivers, along with a digital map to estimate ground vehicles' state is proposed in [9]. However, such a system is applicable to ground vehicles only, expensive to implement, and may not be applicable if a precise digital map is not available. Radar and vision-based systems are also proposed to predict traffic accidents [10]. However, these systems will not be able to provide a 360-degree field of view.

The implementation of vehicle-to-infrastructure communication is suggested in [11]. This approach is suitable for applications aided with real-time traffic data or internet connectivity. However, for collision prediction, communication is only required between vehicles present within the vicinity of each other. Vehicle-to-vehicle communication has the advantage of not requiring an infrastructure. Therefore, it can work in any area where all vehicles are provided with a collision avoidance system along with a compatible communication protocol. In [12], the challenges faced with this implementation are discussed.

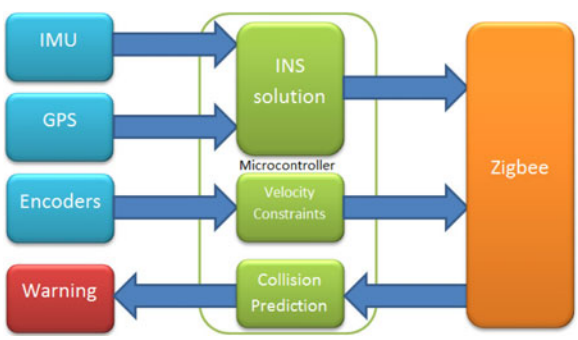

Fig. 1 Overall system architecture

In [13], a navigation solution is proposed using measurements from a gyroscope, GPS receiver, and speedometer. A nonlinear observer that consists of three filters is used in developing a vehicle navigation solution. One of the filters estimates yaw angle and gyro bias. Another filter is used for estimating the speedometer's scaling. The third filter estimates the vehicle's velocity and position. In the filtering stage proposed in [13], nonholomonic constraints are taken into consideration. When tested, the algorithm gave reliable results. However, the algorithm does not take into consideration the accelerometer bias and it also does not use the quaternion approach. The latter quaternion approach is known for its stability in finding a vehicle's attitude.

Constraints are also fused in a navigation solution in [14]. These constraints depend on the orientation of the vehicle relative to the earth and the relationship between the attitude of the vehicle and its velocity. Velocity constraints are also fused with an INS and GPS in [15] for a navigation solution consisting of nine states. The results of this fusion showed that the observability of the attitude of the vehicle is guaranteed. This leads to a decrease in the attitude's estimation errors.

In this work, vehicles' velocity constraints are fused with INS/GPS measurements to enhance the accuracy of state estimation. The state estimation filters are designed for a fifteen state vehicle kinematic model. The velocity constraint measurement is derived based on the utilized model. In addition to the extended Kalman filter, an extended information filter is used to fuse the measurements to reduce the computational complexity of the system. The EIF estimation accuracy is compared to that of the EKF approach to ensure that the state estimate's accuracy is not substantially affected. First, the suggested system's setup is described. The fusion algorithm of the low-cost GPS, velocity constraints, and three-axis gyroscopes and accelerometers is shown next. Experimental results of the estimation algorithm are verified and compared with a standalone commercial solution. Single as well as two-vehicle experimental results are shown in Section 6.

2 System Setup

Figure 1 shows the components of the proposed system. This system is composed of an IMU/GPS unit, a velocity encoder, a Zigbee transceiver, and a microcontroller. The measurements of the IMU and GPS are fused to obtain an estimate of the vehicle's state. The body frame velocity constraint measurement, which is obtained from the airspeed velocity measurement of an UAS or from wheel encoders for ground vehicles, is fused with the GPS/IMU measurements to enhance the accuracy of the estimated state. The microcontroller estimates the state of each vehicle at a 50-Hz rate using the algorithm proposed in this paper. Subsequently, the Zigbee transceiver is responsible for communicating the position, velocity, and attitude to other vehicles in the vicinity.

To estimate the position and velocity of the vehicle, GPS measurements and velocity constraints are fused with measurements from the inertial sensors. The specific force, measured from a three-axis accelerometer, and the angular velocity, measured from a three-axis gyroscope, are integrated to find the vehicle's position, velocity, and attitude. However, due to error accumulation in the INS estimate, the results soon drift away from their actual values. Therefore, GPS measurements are fused with the INS measurements using the EKF to obtain a high-accuracy estimate of the state. In addition, to reduce the computational demand of the algorithm, an EIF is used instead of the EKF for sensor fusion. To enhance the accuracy of the state estimation, velocity constraints are also fused with the GPS/IMU measurements. These constraints improve the results by constraining the body frame y- and z-axis velocities to zero mean with a small magnitude white noise process. The white noise process modeled on the body y and z axes corrects for any possible, small magnitude, side slip of the UAS or ground vehicle.

3 Inertial Navigation System (INS)

The use of accelerometers and gyroscopes to find velocity and position is illustrated in [1–5]. The accelerometer measures the vehicle's specific force vector, F^{b}, in the body frame. The gyroscope provides the vehicle's angular velocity vector, ω^{b}, in the body frame. Here, the superscript b is used to denote the vectors' representation in the body frame. The encoder measures the body frame velocity in the x direction. Also, body frame velocities in the y and z directions are constrained to zero mean with an additive white Gaussian noise. These constraints are known as nonholomonic velocity constraints. Before fusing them with the GPS measurements, the measurements are rotated to the earth centered, earth fixed (ECEF) frame using the transformation matrix C_B^E. In the sections below, the dynamics of the vehicle are described. In the equations to follow, Ω represents the skew matrix of angular velocity of the earth, P is the vehicle's position, V is the vehicle's velocity, and G is the local gravitation vector. The superscript e is used to denote the vectors' representation in the ECEF frame.

3.1 Velocity and Position

The vehicle's dynamics are obtained from the measurements of the accelerometers and gyroscopes. The time rate of change of the velocity with respect to the ECEF frame is given as follows [5]:

$$\dot{V}^e = C_B^E F^b - 2\Omega \mathrm{V}^{\mathrm{e}} - \Omega^2 P^e + G^e \tag{1}$$

To propagate the velocity in the ECEF frame, Eq. 1 is integrated numerically. Subsequently, Eq. 2, shown below, is integrated to find the vehicle's position.

$$\dot{P}^e = V^e \tag{2}$$

Due to the bias error in the accelerometers' specific force, F^{b}, the propagated velocity and position of the vehicle will diverge quickly from the correct position and velocity. The IMU measurements are modeled as follows:

$$\hat{F}^b = F^b - b_a^b - w_a \tag{3}$$

$$\hat{\omega}_{ib}^b = \omega_{ib}^b - b_g^b - w_g \tag{4}$$

$$\dot{b}_a^b = w_{ba} \tag{5}$$

$$\dot{b}_g^b = w_{bg} \tag{6}$$

where $\hat{F}^b$ is the measured vehicle specific force in the body frame, $\hat{\omega}_{ib}^b$ is the measured angular velocity of the vehicle relative to the inertial frame measured in the body frame of the vehicle, b_a^b is the bias in the specific force, b_g^b is the bias in the angular velocity, w_a is the noise on the specific force measurement, w_g is the noise on the angular velocity measurement, w_{ba} is the noise modeling the drift in the bias of specific force, and w_{bg} is the noise modeling the drift in the bias of the angular velocity measurement.

3.2 Attitude

The attitude of the vehicle is represented in quaternion form. In [16], the quaternion algorithm is used to avoid the uncertainty in the vehicle's initial attitude. This algorithm is computed using the computer frame. Also, for the fusion of nonlinear data, the distribution approximation filter (DAF) is used in [17]. The DAF has the advantage of avoiding the complications that are accompanied with calculating Jacobians in the EKF algorithm. This is done by approximating a distribution rather than approximating an arbitrary nonlinear function [18].

The vehicle attitude is therefore represented in the quaternion vector: $q = \begin{bmatrix} q_0 & q_1 & q_2 & q_3 \end{bmatrix}^T$. The time rate of change of the attitude of the vehicle is given in Eq. 7 as:

$$\dot{q}^e = \frac{1}{2}\Omega_{eb}^b q^e \tag{7}$$

given that ω_{eb}^b, the body frame representation of the angular velocity of the vehicle's body frame relative to the ECEF frame, Ω_{eb}^b, is its skew symmetric matrix.

The gyroscope provides the angular velocity of the vehicle, ω_{ib}, relative to the inertial frame. The angular velocity of the earth relative to the inertial frame is subtracted from the angular velocity of the body frame relative to the inertial frame to get the angular velocity of the body relative to the ECEF frame as follows:

$$\omega_{eb} = \omega_{ib} - \omega_{ie} \tag{8}$$

This equation is represented as:

$$\omega_{eb}^b = \omega_{ib}^b - C_E^B \omega_{ie}^e = \begin{bmatrix} \omega_x \\ \omega_y \\ \omega_z \end{bmatrix} \tag{9}$$

And its skew-symmetric cross matrix is represented as:

$$\Omega_{eb}^b = \begin{bmatrix} 0 & -\omega_x & -\omega_y & -\omega_z \\ \omega_x & 0 & \omega_z & -\omega_y \\ \omega_y & -\omega_z & 0 & \omega_x \\ \omega_z & \omega_y & -\omega_x & 0 \end{bmatrix} \tag{10}$$

The quaternions are updated as follows:

$$\hat{q}^e = \delta\hat{q}^e \oplus \bar{q}^e = \begin{bmatrix} \bar{q}_0 & -\bar{q}_1 & -\bar{q}_2 & -\bar{q}_3 \\ \bar{q}_1 & \bar{q}_0 & \bar{q}_3 & -\bar{q}_2 \\ \bar{q}_2 & -\bar{q}_3 & \bar{q}_0 & \bar{q}_1 \\ \bar{q}_3 & \bar{q}_2 & -\bar{q}_1 & \bar{q}_0 \end{bmatrix} \begin{bmatrix} 1 \\ \delta\hat{q}_1 \\ \delta\hat{q}_2 \\ \delta\hat{q}_3 \end{bmatrix} \tag{11}$$

where $\hat{q}^e$ is an estimated quaternion and $\bar{q}^e$ is the a priori estimate of the attitude of the vehicle.

Figure 2 is a block diagram of the proposed navigation algorithm. The top part of the diagram

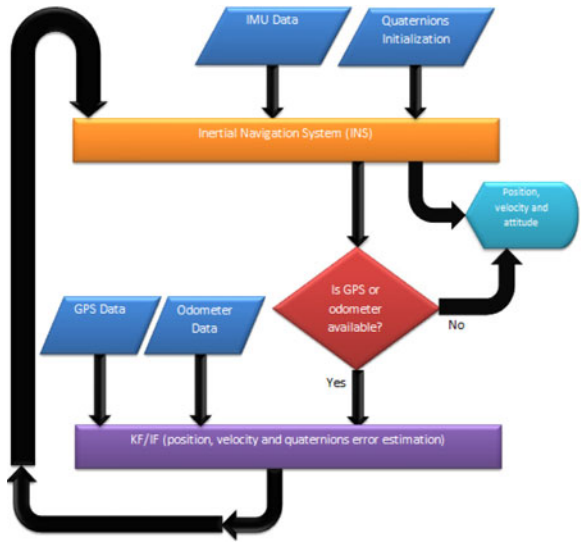

Fig. 2 The constrained INS/GPS navigation algorithm

shows the role of the INS in obtaining the position, velocity, and attitude of the vehicle by integration of the dynamics measured by the IMU. The fusion of the velocity constraint and the GPS measurements with the a priori vehicle state obtained by the INS is shown in the bottom of the figure. The fusion algorithms are described in Section 4. First, the velocity constraint measurement is derived in the next section.

3.3 Velocity Constraint

The body-frame velocity in the y and z axes, v_y^b and v_z^b, are constrained to zero mean with an additional, small-magnitude, white noise. The white noise processes on the x and y axes compensate for any small-magnitude velocities that the vehicle may have along these directions. These velocity constraints are only applied to the model and not to the vehicle's actual dynamics. The fusion of the velocity constraints helps in improving the results of the estimated states. The body frame x-axis velocity measurement, v_x^b, is represented as:

$$z_v^{\text{velocity}}(k) = \begin{bmatrix} v_x^b(k) \\ 0 \\ 0 \end{bmatrix} = C_E^B \mathrm{V}^{\mathrm{e}} + \begin{bmatrix} \eta_x \\ \eta_y \\ \eta_z \end{bmatrix} \tag{12}$$

The measurement equation between the INS readings and the velocity constraint is obtained by first evaluating the above measurement constraint about the nominal, a priori, values as:

$$\bar{\mathrm{V}}^B = C_{\bar{E}}^B \bar{V}^e \tag{13a}$$

But the nominal states are related to the true states as follows:

$$C_{\bar{E}}^B = C_E^B C_{\bar{E}}^E \tag{13b}$$

$$\mathrm{V}^e = \bar{V}^e - \delta \mathrm{V}^e \tag{13c}$$

Therefore, by substituting Eqs. 13a, 13b, and 13c in Eq. 12, we obtain:

$$z_v^{\text{velocity}}(k) = C_{\bar{E}}^B C_E^{\bar{E}} \left(\bar{V}^{\mathrm{e}} - \delta \mathrm{V}^e\right) + \begin{bmatrix} \eta_x \\ \eta_y \\ \eta_z \end{bmatrix} \tag{14}$$

and with the error in the cosine matrix, assuming small attitude error, represented as $C_E^{\bar{E}} = \left(I - 2\left[\delta q^e\right]^\times\right)$, Eq. 14 is written as:

$$z_v^{\text{velocity}}(k) = C_{\bar{E}}^B \left(I - 2\left[\delta q^e\right]^\times\right)\left(\bar{V}^{\mathrm{e}} - \delta \mathrm{V}^e\right) + \begin{bmatrix} \eta_x \\ \eta_y \\ \eta_z \end{bmatrix} \tag{15}$$

Expanding the terms in Eq. 15:

$$z_v^{\text{velocity}}(k) = C_{\bar{E}}^B \bar{V}^{\mathrm{e}} - C_{\bar{E}}^B \delta \mathrm{V}^e - 2C_{\bar{E}}^B \left[\delta q^e\right]^\times \bar{V}^{\mathrm{e}} + 2C_{\bar{E}}^B \left[\delta q^e\right]^\times \delta \bar{V}^{\mathrm{e}} + \begin{bmatrix} \eta_x \\ \eta_y \\ \eta_z \end{bmatrix} \tag{16}$$

The term $2C_{\bar{E}}^B \left[\delta q^e\right]^\times \delta \bar{V}^{\mathrm{e}}$ is assumed to be negligible to the first order. Also, by substituting:

$$2C_{\bar{E}}^B \left[\delta q^e\right]^\times \bar{V}^{\mathrm{e}} = -2C_{\bar{E}}^B \left[\bar{V}^{\mathrm{e}}\right]^\times \delta q^e$$

Equation 16 can be written as:

$$z_v^{\text{velocity}}(k) = C_{\bar{E}}^B \bar{V}^{\mathrm{e}} - C_{\bar{E}}^B \delta \mathrm{V}^e + 2C_{\bar{E}}^B \left[\bar{V}^{\mathrm{e}}\right]^\times \delta q^e + \begin{bmatrix} \eta_x \\ \eta_y \\ \eta_z \end{bmatrix} \tag{17}$$

By subtracting Eq. 17 from Eq. 13a, the following is obtained:

$$\bar{V}^B - z_v^{\text{velocity}}(k) = C_{\bar{E}}^B \delta \mathrm{V}^e - 2C_{\bar{E}}^B \left[V^{\mathrm{e}}\right]^\times \delta q^e + \begin{bmatrix} \eta_x \\ \eta_y \\ \eta_z \end{bmatrix} \tag{18}$$

with $\bar{V}^B = z_v^{INS}(k)$, the constraint measurement equation, written as:

$$z_v^{INS}(k) - z_v^{\text{velocity}}(k) = C_{\bar{E}}^B \delta \mathrm{V}^e - 2C_{\bar{E}}^B \left[\bar{V}^{\mathrm{e}}\right]^\times \delta q^e + \begin{bmatrix} \eta_x \\ \eta_y \\ \eta_z \end{bmatrix} \tag{19}$$

Therefore, the velocity constraint measurement matrix is given as:

$$H_v^{\text{velocity}}(k) = \begin{bmatrix} 0 & C_{\bar{E}}^B & -2C_{\bar{E}}^B \left[\bar{V}^{\mathrm{e}}\right]^\times & 0 & 0 \end{bmatrix} \tag{20}$$

The covariance of the velocity constraint measurement error is represented as:

$$R_v^{\text{velocity}}(k) = \begin{bmatrix} \sigma_x^2 & 0 & 0 \\ 0 & \sigma_y^2 & 0 \\ 0 & 0 & \sigma_z^2 \end{bmatrix} \tag{21}$$

To eliminate the propagated bias in position, velocity, and attitude estimates, an EKF and EIF are used to fuse the measurements of the GPS, velocity constraint, and a priori vehicle's estimates obtained from the integration of the gyroscopes and accelerometers.

4 Measurement Fusion Algorithm Using EKF

The Kalman filter estimates vehicle position, velocity, and attitude by fusing the GPS and velocity constraint with the a priori INS-propagated estimates.

The error state vector used is described as:

$$x = \begin{bmatrix} \delta P^e & \delta V^e & \delta q^e & \delta b_a^b & \delta b_g^b \end{bmatrix}^T \tag{22}$$

Performing perturbation analysis using Eqs. 1–7, the dynamics of this error state can be obtained and represented in vector form as [3]:

$$\dot{x} = Ax + Bw \tag{23}$$

where

$$A = \begin{bmatrix} 0 & I & 0 & 0 & 0 \\ \nabla \bar{G}^e - \Omega^2 & -2\Omega & -2\left[C_{\bar{B}}^{\bar{E}} F^b\right]^X & C_{\bar{B}}^{\bar{E}} & 0 \\ 0 & 0 & -\Omega & 0 & \frac{1}{2} C_{\bar{B}}^{\bar{E}} \\ 0 & 0 & 0 & 0 & 0 \\ 0 & 0 & 0 & 0 & 0 \end{bmatrix},$$

$$B = \begin{bmatrix} 0 & 0 & 0 & 0 \\ C_{\bar{B}}^{\bar{E}} & 0 & 0 & 0 \\ 0 & \frac{1}{2} C_{\bar{B}}^{\bar{E}} & 0 & 0 \\ 0 & 0 & I & 0 \\ 0 & 0 & 0 & I \end{bmatrix},$$

and $w = \begin{bmatrix} w_a \\ w_g \\ w_{ba} \\ w_{bg} \end{bmatrix}$.

The dynamic Eq. 23 is descritized to obtain:

$$x(k) = A(k)x(k-1) + B(k)\, w(k) \tag{24}$$

Initial calibration of the IMU is performed to minimize the magnitude of the state error in the propagation stage [1]. At the start of operation, $x(1|0)$ is set to zero and initial position, velocity, and attitude are obtained from the GPS and compass. Subsequently, the dynamics Eqs. 1–8 are integrated numerically to obtain the state of the vehicle when GPS measurements are not available. During this stage, the error in the state will accumulate due to the bias error in the IMU. Also, the covariance of the propagated state will grow with time due to the noise-driven dynamics Eq. 24. The covariance matrix, $P(k|k-1)$, is propagated in time as:

$$P(k|k-1) = A(k)\, P(k-1|k-1)\, A^T(k) + Q(k) \tag{25}$$

where $Q(k)$ is the process noise covariance matrix at time k. Therefore, to reduce the error in the propagated state estimate, the error measurement is used to update the state using the EKF. The error measurement used is given as:

$$z(k) = \begin{bmatrix} z_p^{INS}(k) - z_p^{GPS}(k) \\ z_v^{INS}(k) - z_v^{GPS}(k) \\ z_v^{INS}(k) - z_v^{\text{velocity}}(k) \end{bmatrix} \tag{26}$$

Using an EKF, the error estimate is updated every time step using the following equation:

$$\hat{x}(k|k) = \hat{x}(k|k-1) + W(k)\nu(k) \tag{27}$$

$W(k)$ is a Kalman gain matrix and $\nu(k)$ is the innovation matrix. These are obtained as:

$$W(k) = P(k|k-1)\, H^T(k) S^{-1}(k) \tag{28}$$

$$\nu(k) = z(k) - H(k)\, \hat{x}(k|k-1) \tag{29}$$

The matrix, $S(k)$, which is known as the innovation covariance, is propagated as:

$$S(k) = H(k)\, P(k|k-1)\, H^T(k) + R(k) \tag{30}$$

where R(k) is the covariance of the measurements' noise at time k. The covariance matrix is updated as:

$$P(k|k) = (I - W(k)\,H(k))\,P(k|k-1) \times (I - W(k)\,H(k))^T + W(k)\,R(k)\,W^T(k) \quad (31a)$$

where

$$H(k) = \begin{bmatrix} I & 0 & 0 & 0 & 0 \\ 0 & I & 0 & 0 & 0 \\ 0 & C_{\bar{E}}^{B} & -2C_{\bar{E}}^{B}\left[\bar{V}^{e}\right]^{\times} & 0 & 0 \end{bmatrix} \quad (31b)$$

and

$$R^{GPS}(k) = \begin{bmatrix} R_P^{GPS} & 0 & 0 \\ 0 & R_v^{GPS} & 0 \\ 0 & 0 & R_v^{\text{velocity}} \end{bmatrix} \quad (31c)$$

where, in Eqs. 31b and 31c, 0 is a 3×3 matrix of zeros and I is a 3×3 identity matrix.

Once the state is updated using Eq. 27, the cosine rotation matrix, $C_B^{\bar{E}}$, is updated to obtain C_B^E using Equation [3]:

$$C_B^{\bar{E}} = C_E^{\bar{E}} C_B^E \quad (32a)$$

where $C_E^{\bar{E}}$ is the error in $C_B^{\bar{E}}$ computation and is represented, assuming small error, as

$$C_E^{\bar{E}} = \left(I - 2\left[\delta q^e\right]^{\times}\right) \quad (32b)$$

δq^e is the attitude between E and $\bar{E}$ frame and is represented as

$$\delta q^e = \begin{bmatrix} \delta q_1 \\ \delta q_2 \\ \delta q_3 \end{bmatrix} \quad (32c)$$

Therefore,

$$C_B^{\bar{E}} = \left(I - 2\left[\delta q^e\right]^{\times}\right) C_B^E \quad (32d)$$

To reduce the computational requirement of the EKF formulation, the fusion of the measurements and dynamics based on an information filter formulation is introduced.

5 Measurement Fusion Algorithm Using EIF

Theoretically, the EIF should give the same result as the EKF. However, the EIF is computationally easier to apply when measurements from multiple sensors are fused. This is because it uses the information space rather than the state space.

The main components of the information filter are the information state matrix and the information state vector. The information state matrix, which is the inverse of the covariance matrix, is given as:

$$Y(k) = P^{-1}(k) \quad (33a)$$

and the information state vector is represented as:

$$y(k) = Y(k)\,x(k) \quad (33b)$$

The a priori information state matrix is given as:

$$\hat{Y}(k|k-1) = \left[A(k)\,\hat{Y}(k-1|k-1)\,A^T(k) + Q(k)\right]^{-1} \quad (34a)$$

while the a priori information vector is evaluated as

$$\hat{y}(k|k-1) = P^{-1}(k-1|k-1)\,A(k) \times P(k-1|k-1) \times \hat{y}(k-1|k-1) \quad (34b)$$

The contribution of the observation is represented in the information observation vector as:

$$i(k) = H^T(k)\,R^{-1}(k)\,z(k) \quad (35a)$$

and the information observation matrix, $I(k)$, that represents the certainty, is given as:

$$I(k) = H^T(k)R^{-1}(k)H(k) \quad (35b)$$

The information observation vector and the information observation matrix are evaluated when an observation $z(k)$ is available. The estimates are updated as

$$\hat{y}(k|k) = \hat{y}(k|k-1) + i(k) \quad (36a)$$

$$\hat{Y}(k|k) = \hat{Y}(k|k-1) + I(k) \quad (36b)$$

For multiple sensors, the estimates are updated by adding the summation of the information observation vectors and matrices for the multiple sensors used as follows:

$$\hat{y}(k|k) = \hat{y}(k|k-1) + \sum i(k) \tag{37a}$$

$$\hat{Y}(k|k) = \hat{Y}(k|k-1) + \sum I(k) \tag{37b}$$

The recursive update algorithm of the EIF, as seen in the above equations, makes its use advantageous for real-time applications. This is because it requires less computational demand than the EKF approach. By fusing the dynamics of the vehicle measured by the accelerometers and gyroscopes with the GPS measurements and the velocity constraints, the errors in the estimates of position, velocity, and attitude are reduced.

6 Experimental Testing

The algorithms presented in this paper were implemented in code and tested. Multiple experiments were conducted to test the performance of the proposed algorithms. First, a static test was performed. Results of this experiment should give zero velocity and constant position. This experiment was used for tuning statistics of the sensors' noise processes and validating the accuracy of the proposed estimation filters. Subsequently, various dynamic experiments were conducted. Vehicles were driven around various trajectories and the proposed algorithms were used to estimate the state of the vehicle. Results obtained from these experiments are shown below. In the results below, the estimated state obtained from the proposed algorithms (green line) is validated against a commercial off-the-shelf (COTS) MIDG solution (blue line) [19].

6.1 Single-Vehicle Dynamic Test Using EKF Without Velocity Constraints

Figures 3, 4, 5, 6, 7 and 8 give the results of a single-vehicle dynamic test when the vehicle was driven around the path shown in Fig. 3. The results were obtained using the EKF without using the velocity constraints. As seen from the figures, the estimates closely follow the results from the MIDG overall. However, since the velocity constraints measurement is not used, it is expected that both the EKF solution and the MIDG solution are biased from the vehicle's true path.

Figure 4 shows that the y and z components of the velocity estimate follow those of the MIDG, which are not close to zero. Figures 5 and 6 show the normal Gaussian distributions of the ECEF position error and body-frame velocity error, respectively. The errors are computed by

Fig. 3 Path estimate of the vehicle, dynamic test using EKF without velocity constraints

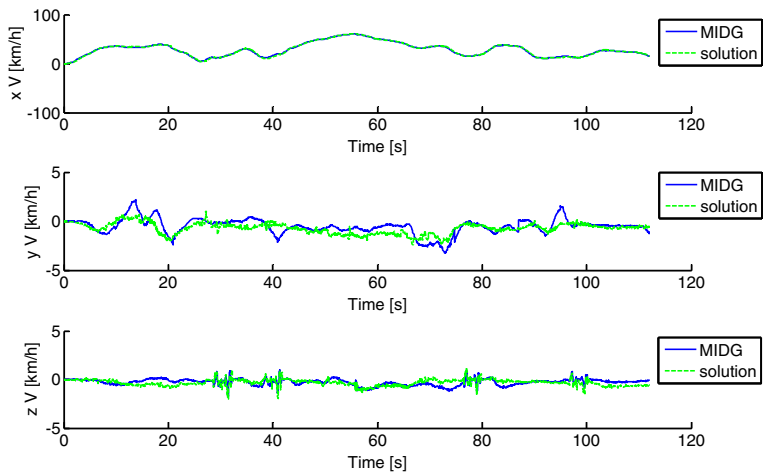

Fig. 4 Velocity estimate, dynamic test using EKF without velocity constraints

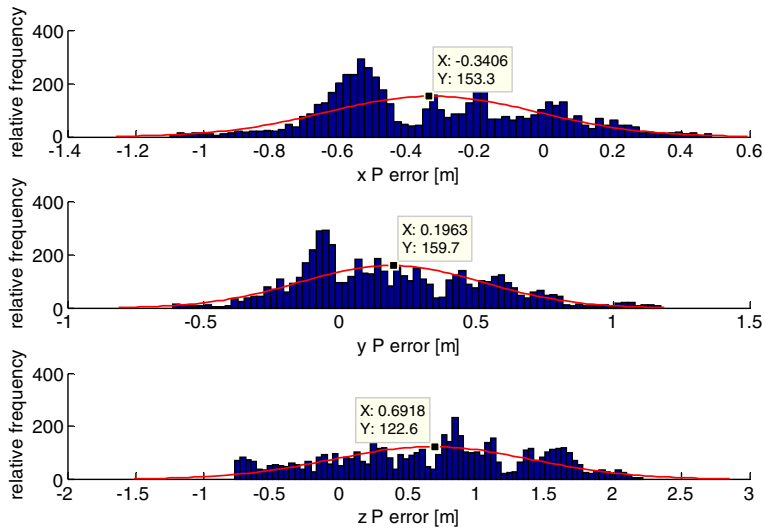

Fig. 5 Position error in ECEF frame, dynamic test using EKF without velocity constraints

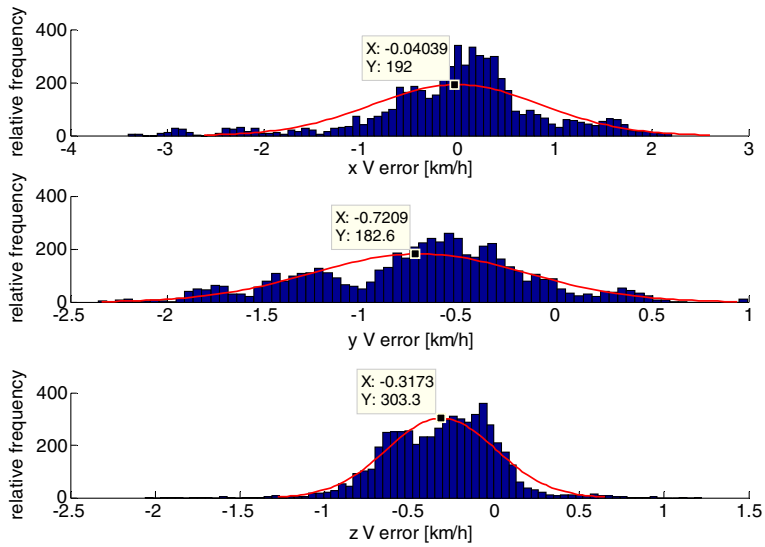

Fig. 6 Velocity error in body frame, dynamic test using EKF without velocity constraints

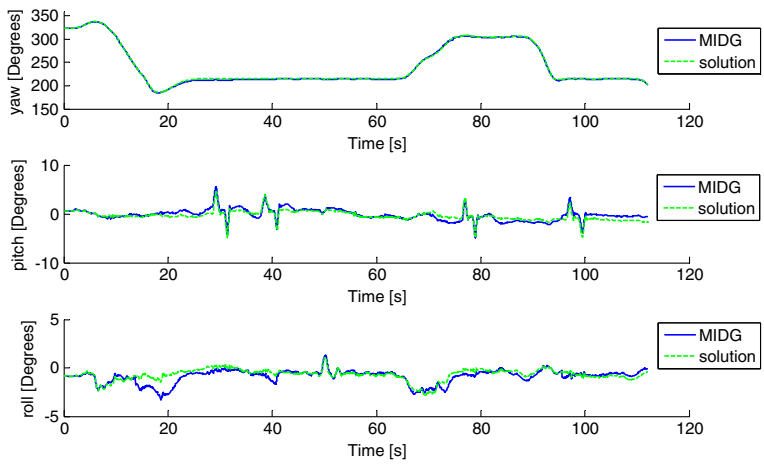

Fig. 7 Attitude estimate, dynamic test using EKF without velocity constraints

subtracting the position and velocity estimates from those given by the MIDG solution. From Fig. 5, it can be noticed that the position errors in the body frame are, on average, less than −0.8 to 0.4 m for the x direction, between −0.5 and 1 m in the y direction, and between −0.8 and 2 m in the z direction. Figure 5 shows that the mean of error in the body-frame x-axis position estimate is around 0.3 m. A velocity error of around −0.04 km/h in the body frame x axis, −0.72 km/h in the body frame y axis, and −0.32 km/h in the body frame z axis are seen from Fig. 6.

Figures 7 and 8 show the absolute and the error in the vehicle's attitude, respectively. The change of the yaw angle during the first 20 s, shown in Fig. 7, indicates that the vehicle was travelling along a roundabout. It is clear that the estimate of the yaw angle provided by the solution follows the yaw angle provided by the MIDG unit despite the highly involved dynamics of the vehicle in the first 20 s and the two turns at around the 70th and 90th s of the test. Figure 8 shows that the errors in yaw, pitch, and roll have means of around 0.65, −0.14, and 0.16 degrees, respectively.

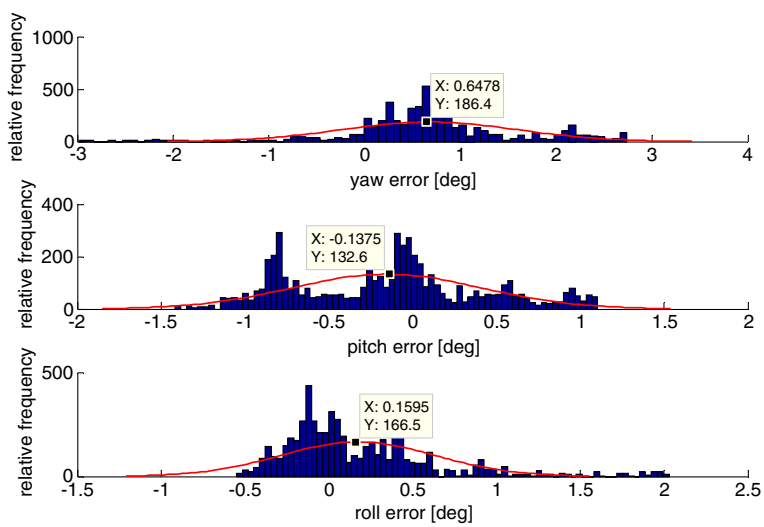

Fig. 8 Attitude error, dynamic test using EKF without velocity constraints

Fig. 9 Path estimate of the vehicle, dynamic test using EKF with velocity constraints

6.2 Single-Vehicle Dynamic Test Using EKF with Velocity Constraints

In Figs. 9, 10 and 11, the vehicle's estimated path, velocity (in body frame), and position (in ECEF) estimated using the EKF with velocity constraints are shown and compared against the MIDG solution. Figure 9 shows that the path of the vehicle estimated by the EKF closely matches the MIDG solution. Similarly, it can be seen from Fig. 10 that the velocity estimates closely match the MIDG solution. The estimated velocity of the vehicle in the body y and z axes are closer to zero than those reported by the MIDG solution. This is true for this ground vehicle experiment. Along this experiment, the vehicle drove over four bumps as seen in Fig. 10 around the 30th, 40th, 78th, and 98th s.

From Fig. 11, it can be noticed that the mean of the position errors in the ECEF frame is around −0.18 m for the x direction, less than −0.76 m for the y direction, and 0.90 m for the z direction. Figure 12 shows that the mean of the velocity error is around 0 km/h. This shows an improvement in the error compared to the results obtained using the EKF without velocity constraints.

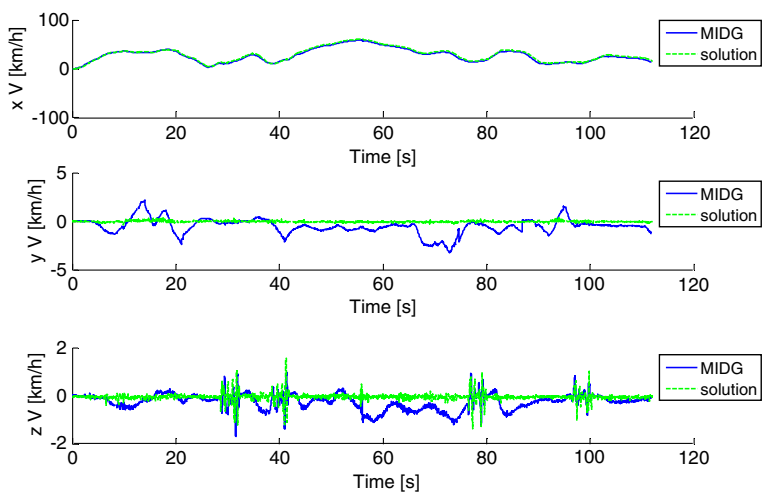

Fig. 10 Velocity estimate, dynamic test using EKF with velocity constraints

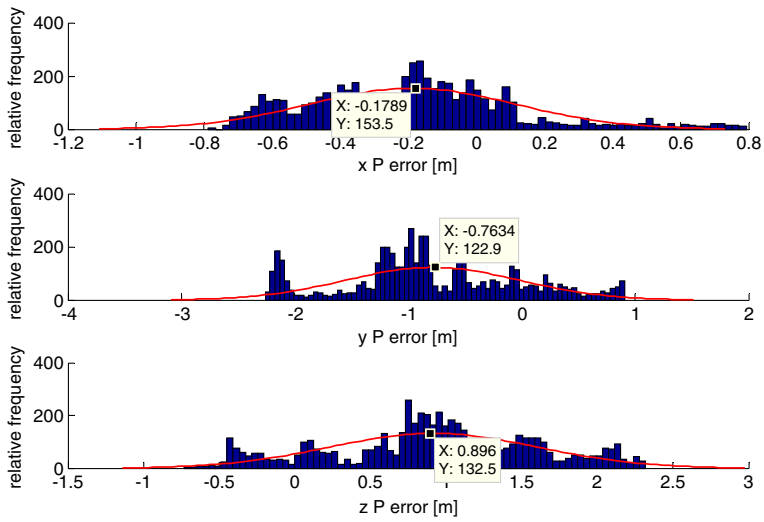

Fig. 11 Position error in ECEF frame, dynamic test using EKF with velocity constraints

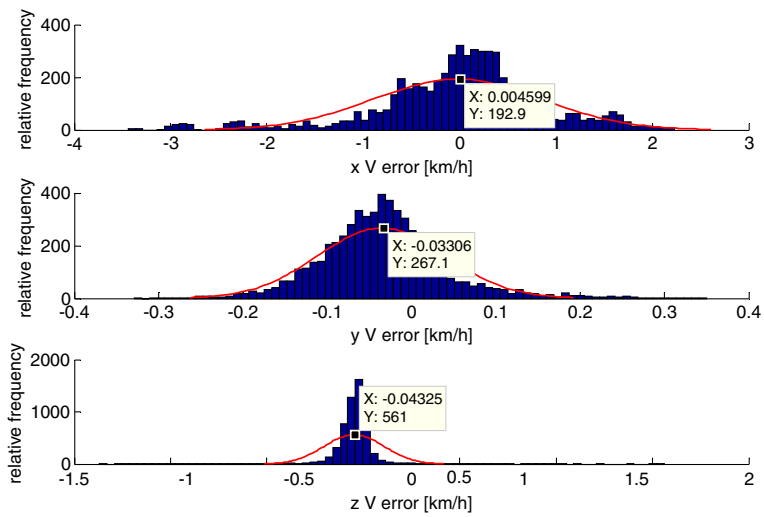

Fig. 12 Velocity error in body frame, dynamic test using EKF with velocity constraints

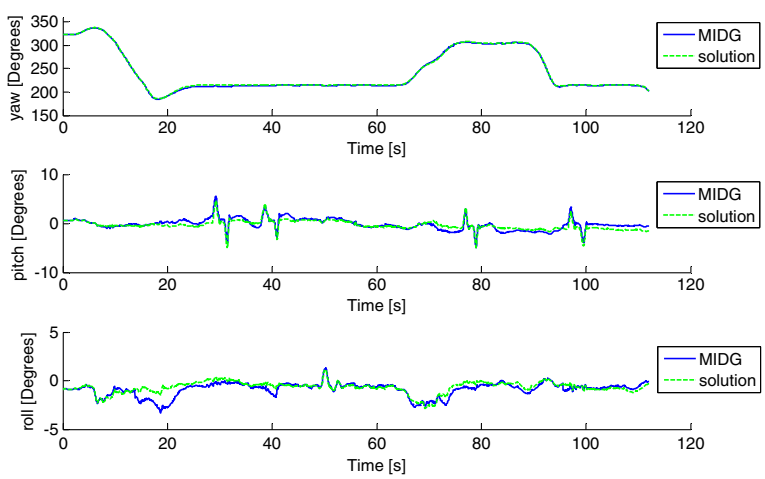

Fig. 13 Attitude estimate, dynamic test using EKF with velocity constraints

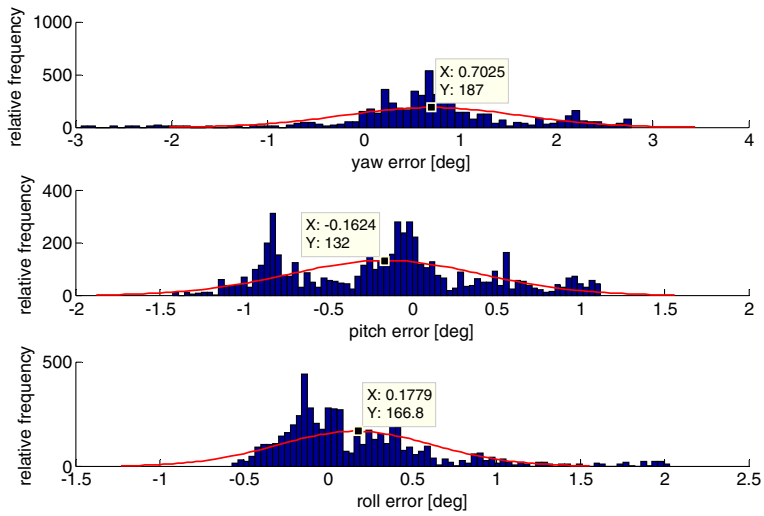

Fig. 14 Attitude error, dynamic test using EKF with velocity constraints

Fig. 15 Path estimate of the vehicle, dynamic test using EIF with velocity constraints

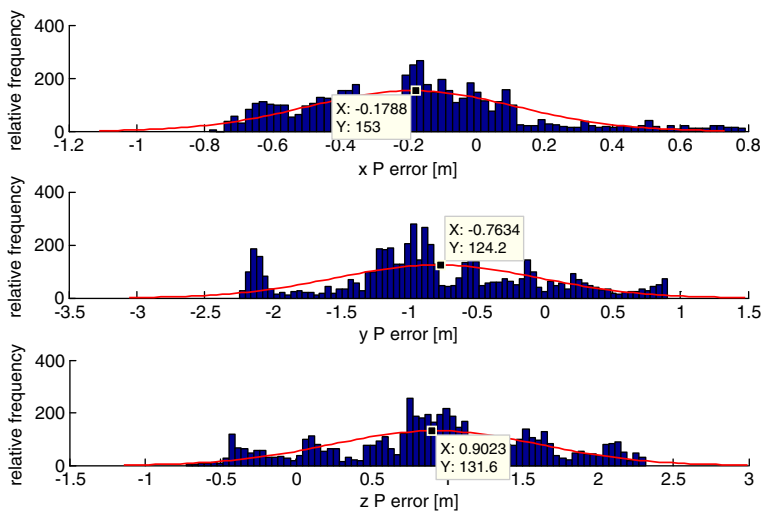

Fig. 16 Position error in ECEF frame, dynamic test using EIF with velocity constraints

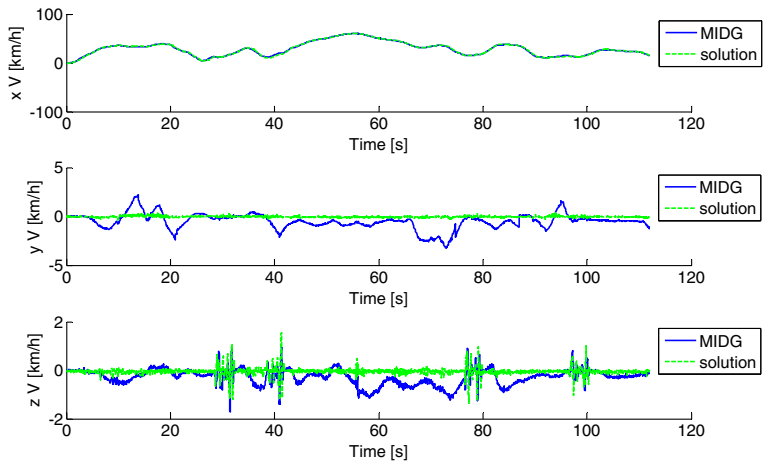

Fig. 17 Velocity estimate, dynamic test using EIF with velocity constraints

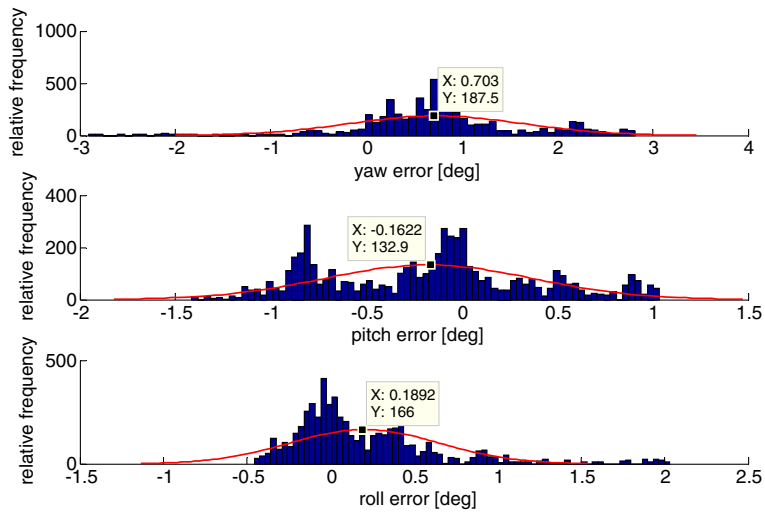

Fig. 18 Attitude error, dynamic test using EIF with velocity constraints

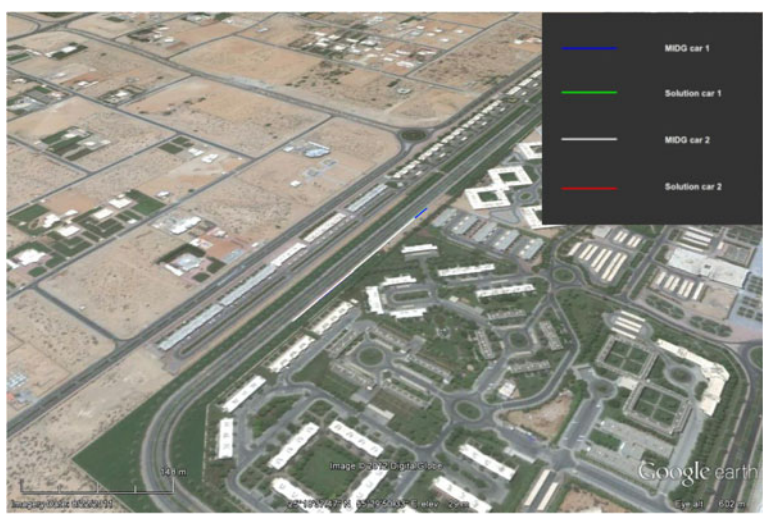

Fig. 19 Path estimates of the vehicles, two-vehicle dynamic test 1 using KF with velocity constraints

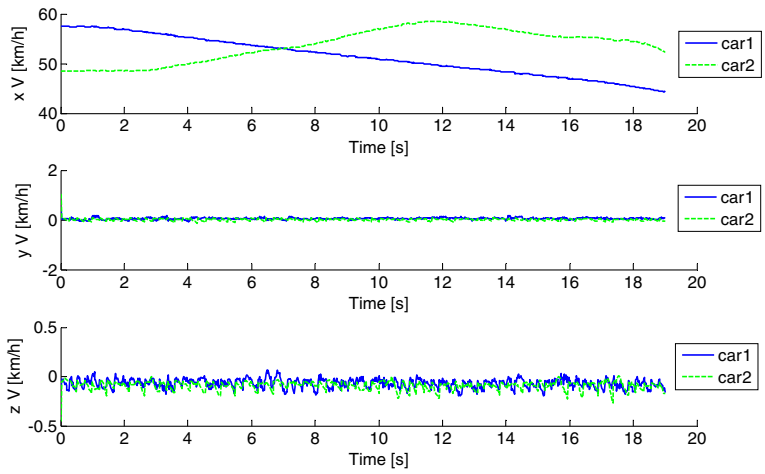

Fig. 20 Velocity estimate, two-vehicle dynamic test 1 using the EKF with velocity constraints

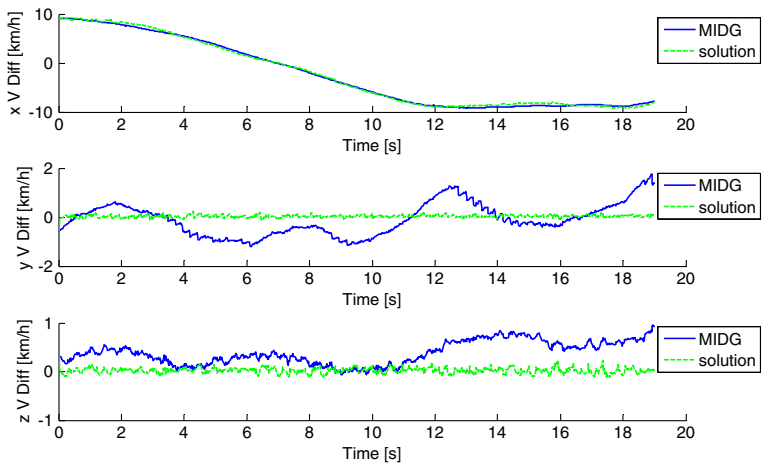

Fig. 21 Vehicle 2 velocity relative to vehicle 1 velocity in test 1 using KF with velocity constraints

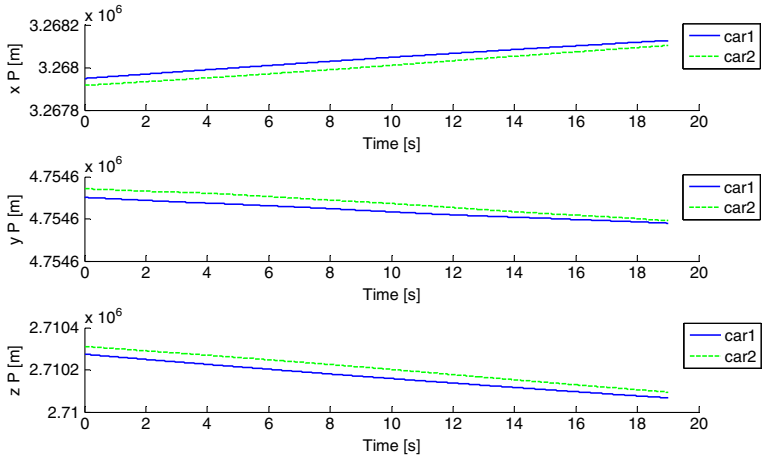

Fig. 22 Position estimate, two-vehicle dynamic test 1 using EKF with velocity constraints

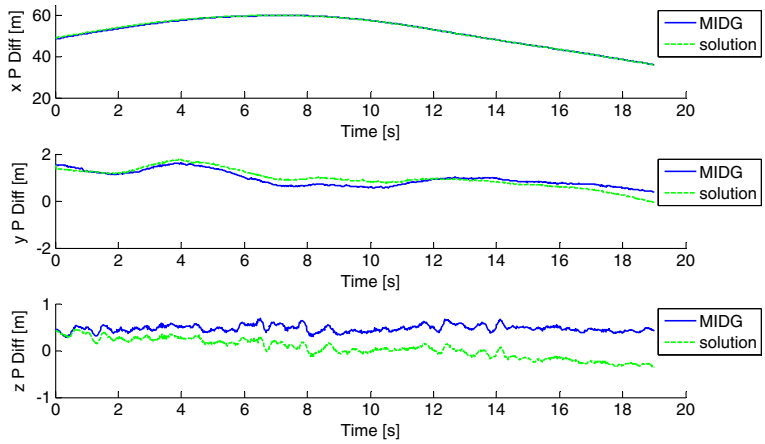

Fig. 23 Vehicle 2 position relative to vehicle 1 position in test 1 using EKF with velocity constraints

Figure 13 shows the attitude estimate of the vehicle. The peaks in the estimated pitch angle again show that the vehicle passed over 4 bumps around seconds 30, 40, 78, and 98. The normal distribution of the error in the vehicle's attitude estimate shown in Fig. 14 demonstrates the ability of the algorithm to accurately estimate the vehicle's attitude as the errors are close to zero degrees in yaw, pitch, and roll.

6.3 Single-Vehicle Dynamic Test Using EIF with Velocity Constraints

In this section, the dynamics of the vehicle, obtained from the IMU, are fused with the GPS and encoder data using the extended information filter. The results of this experiment are shown in Figs. 15, 16, 17 and 18.

Figure 15 shows that the EIF accurately estimates the position of the vehicle. This is confirmed in Fig. 16 as the ECEF frame position error is around −0.18 m, −0.76 m, and 0.90 m along the x, y and z axes. It can be seen from Fig. 17 that velocities closer to zero, in comparison to the MIDG solution, are obtained in the body frame y and z axes.

Figure 18 shows the error in the attitude estimate obtained using the EIF. The figure shows that the algorithm accurately estimates the vehicle's attitude.

Next, the results of multiple vehicle tests are shown and discussed.

6.4 Two-Vehicle Dynamic Test 1 Using EKF with Velocity Constraints

The proposed EKF filter was implemented on two vehicles that were driven simultaneously around a trajectory. Figures 19, 20, 21, 22, 23, 24, 25 and 26 show the results obtained from this two-vehicle dynamic test. Figure 19 shows the path estimates of the two vehicles using the MIDG and the EKF. In this test, vehicle 2 was following vehicle 1. The different lines in Fig. 19 are not all visible because of path overlap.

Figures 20 and 21 show the velocities of both vehicles in the body frame, and the velocity of vehicle 2 relative to that of vehicle 1 represented

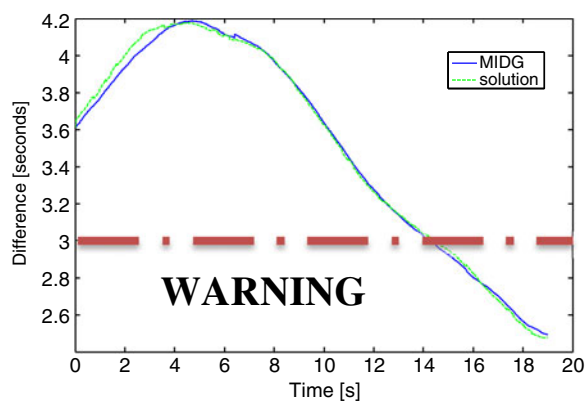

Fig. 24 Lagging of vehicle 2 behind vehicle 1 in seconds using EKF with velocity constraints

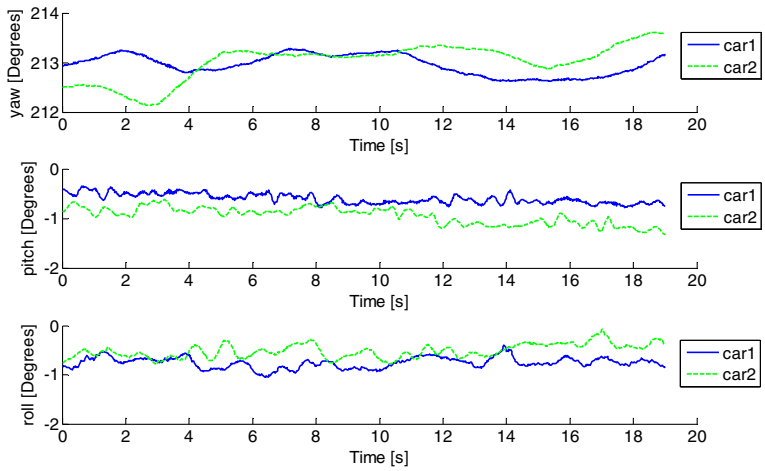

Fig. 25 Attitude estimate, two-vehicle dynamic test 1 using EKF with velocity constraints

in the body frame of vehicle 2, respectively. It can be noticed that during the first 7 s of the test, the forward velocity of vehicle 1 was more than that of vehicle 2. After that, the forward velocity of vehicle 2 exceeded that of vehicle 1 as shown in Fig. 21.

Figure 22 shows the position of the two vehilces in the ECEF frame while Fig. 23 shows the position of vehicle 2 relative to vehilces 1 represented in the body frame of vehicle 2. Figure 23 shows that vehilces 2 was lagging behind vehilces 1 with around 49 m at the beginning, around 60 m at the seventh second, and around 36 m at the end of the test.

To determine the time vehicle 2 was lagging behind vehicle 1 in seconds, the distance between the two vehicles in meters is divided by the forward velocity of the lagging vehicle as:

$$\text{Difference in seconds} = \frac{P_1^{bx} - P_2^{bx}}{V_2^{bx}} \tag{38}$$

Figure 24 shows this relative time between vehicle 2 and vehicle 1.

Figure 24 demonstrates that vehilce 2 was lagging behind vehilce 1 with about 3.6 s at the beginning of the test, about 4.2 s at the fifth second, and around 2.5 s at the end of the test. Therefore,

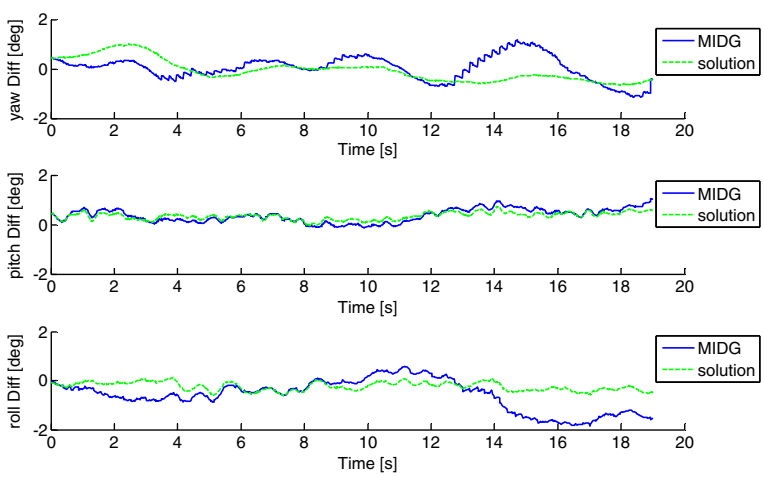

Fig. 26 Vehicle 2 attitude relative to vehicle 1 attitude in test 1 using EKF with velocity constraints

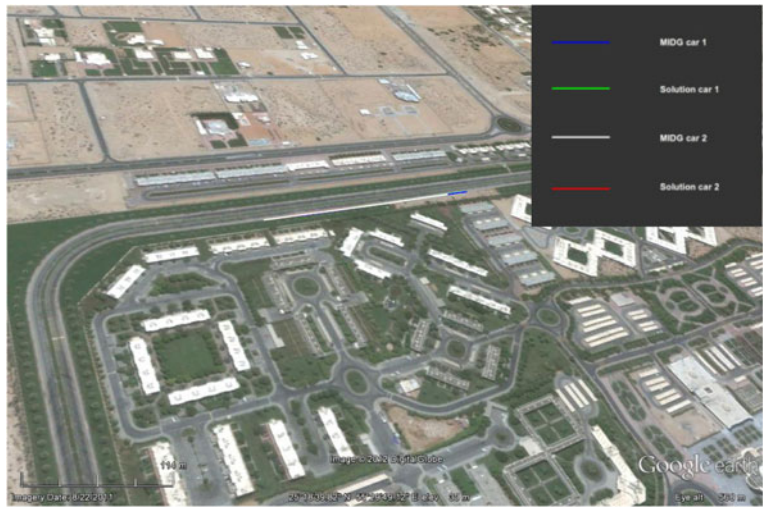

Fig. 27 Path estimates of the vehicles, two-vehicle dynamic test 1 using EIF with velocity constraints

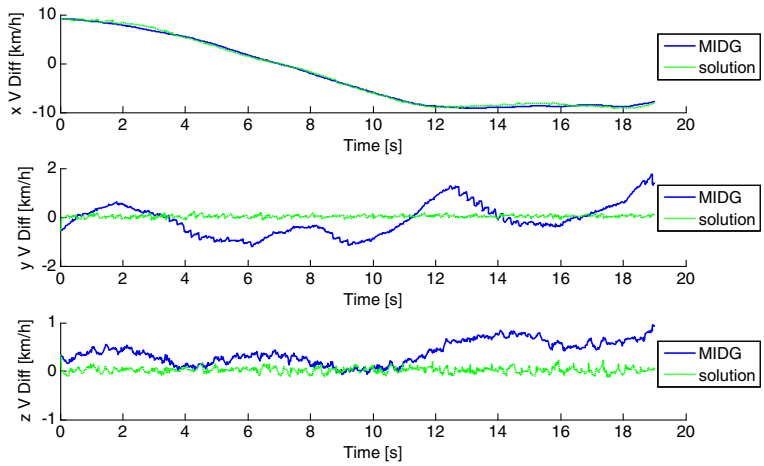

Fig. 28 Vehicle 2 velocity relative to vehicle 1 velocity in test 1 using EIF with velocity constraints

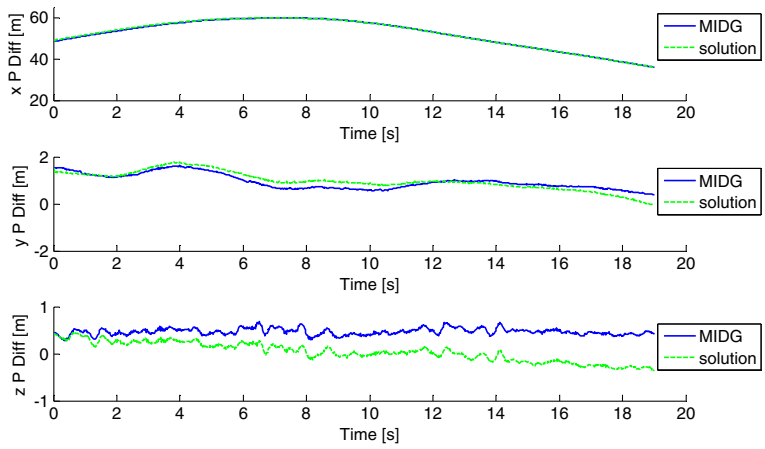

Fig. 29 Vehicle 2 position relative to vehicle 1 position in test 1 using EIF with velocity constraints

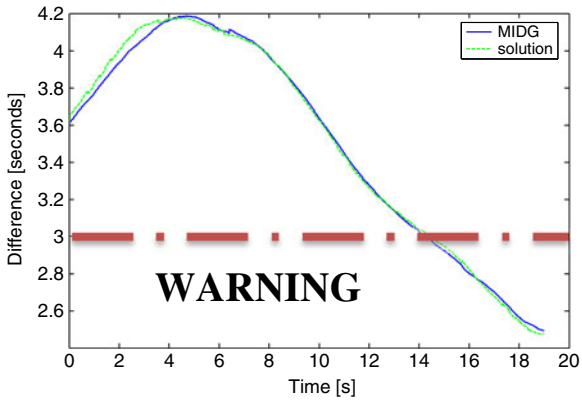

Fig. 30 Lagging of vehicle 2 behind vehicle 1 in seconds using EIF with velocity constraints

at the fourteenth second of the test, a warning line of 3 s was crossed. As a result, a warning can be issued to the driver.

Figures 25 and 26 show the attitude of the two vehicles and the attitude of vehilce 2 relative to vehilce 1, respectively. From Fig. 25, it can be noticed that the difference in yaw is close to zero degrees, which shows that the two vehicles were travelling in the same direction. Therefore, the warning must also be conditioned with this fact keeping in mind that the distance between the two vehicles in the y axis is less than 2 m, as shown in Fig. 23, which indicates that the two vehicles are in the same lane.

6.5 Two-Vehicle Dynamic Test 1 Using EIF with Velocity Constraints

Figures 27, 28, 29, 30 and 31 show the results for the same previous two-vehicle dynamic test, except this time the results were processed using the EIF. The proposed EIF algorithm was implemented onboard each vehicle. Figure 19 shows the path estimates of the two vehicles using the MIDG and the EIF. The different lines in Fig. 27 are not all visible because of path overlap.

Figure 28 shows the relative velocity between vehicle 2 and vehicle 1 in the body frame of vehicle 2. It can be noticed that at the beginning, the forward velocity of vehicle 2 was more than that of vehicle 1. At around the seventh second of the test, the forward velocity of vehicle 1 exceeded that of vehicle 2.

Figure 29 shows the position of vehicle 2 relative to vehicle 1 in the body frame of vehicle 2. The figure shows that vehicle 2 was following vehicle 1 throughout the entire test.

Figure 30 shows this relative time between vehicle 2 and vehicle 1 obtained using Eq. 38. The time separation between the two vehicles is in agreement with that obtained using the EKF in Fig. 24.

Figure 31 shows the relative attitude of vehicle 2 relative to vehicle 1. It is noticed that the difference in yaw is close to zero degrees, which shows that the two vehicles were travelling in the same direction for the entire test.

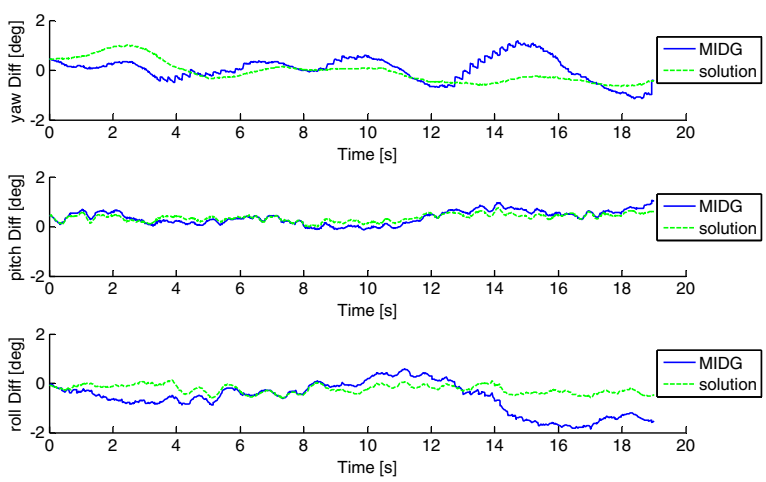

Fig. 31 Vehicle 2 attitude relative to vehicle 1 attitude in test 1 using EIF with velocity constraints

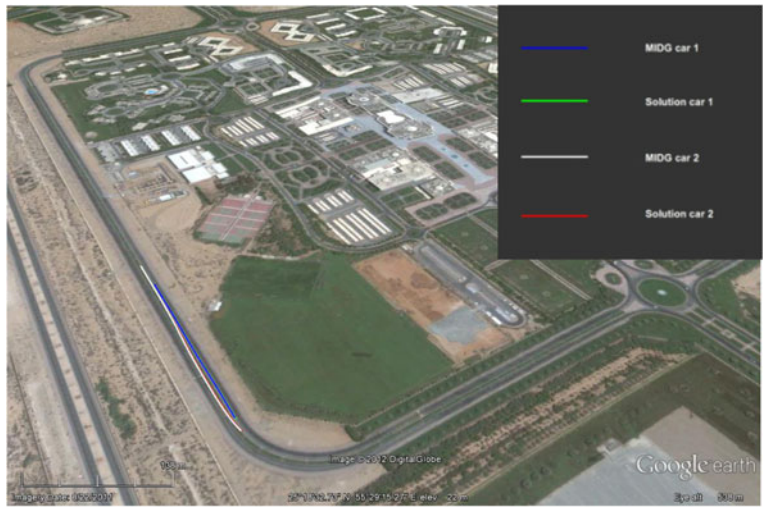

Fig. 32 Path estimates of the vehicles, two-vehicle dynamic test 2 using EIF with velocity constraints

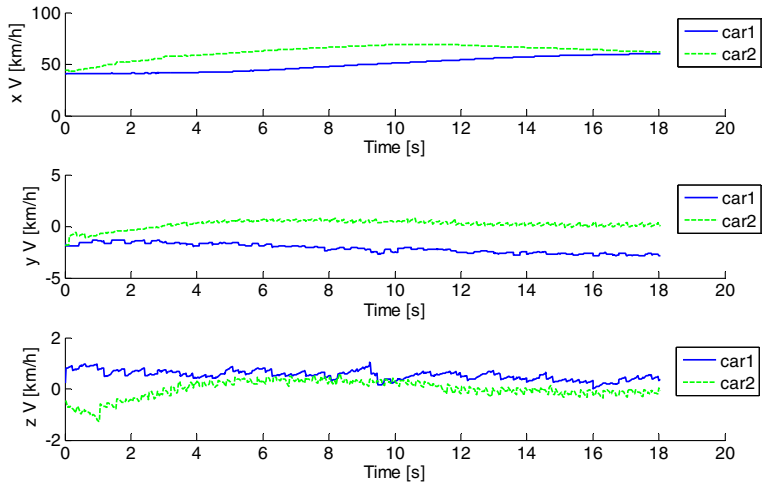

Fig. 33 Velocity estimate, two-vehicle dynamic test 2 using EIF with velocity constraints

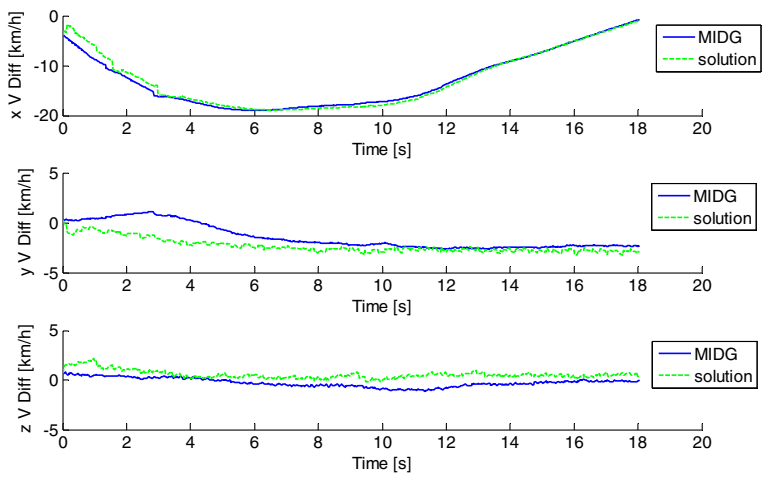

Fig. 34 Vehicle 2 velocity relative to vehicle 1 velocity in test 2 using EIF with velocity constraints

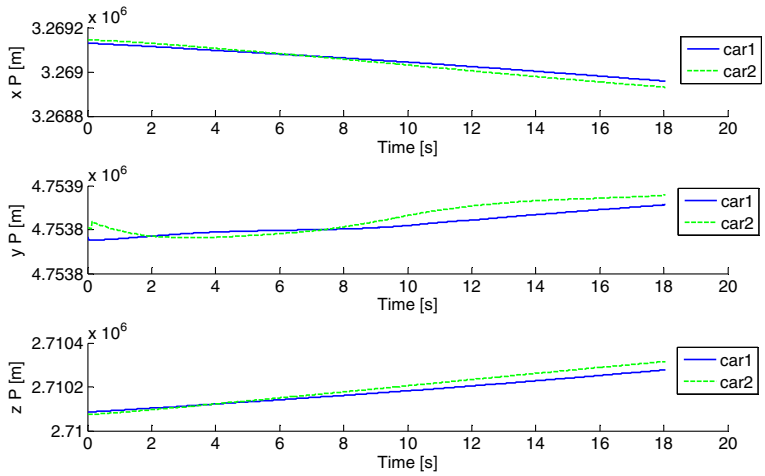

Fig. 35 Position estimates, two-vehicle dynamic test 2 using EIF with velocity constraints

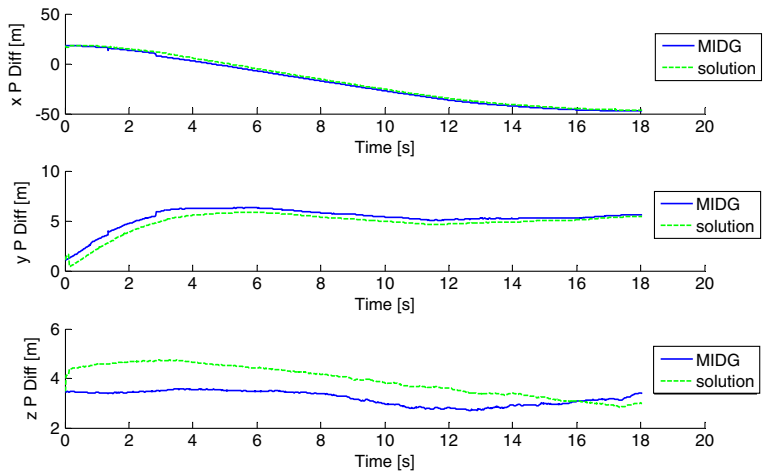

Fig. 36 Vehicle 2 position relative to vehicle 1 velocity in test 2 using EIF with velocity constraints

The results obtained using the EIF were very close to those that were obtained in the previous section using the EKF.

6.6 Two-Vehicle Dynamic Test 2 Using EIF with Velocity Constraints

Figures 32, 33, 34, 35, 36, 37, 38 and 39 show the results of a two-vehicle test where one vehicle overtakes the other vehicle during the experiment. The estimated path of the two vehicles is shown in Fig. 32.

Figures 33 and 34 show the velocities of both vehicles in body frame and the forward velocity of vehicle 2 relative to vehicle 1 represented in vehicle 2's body frame, respectively. From Fig. 33,

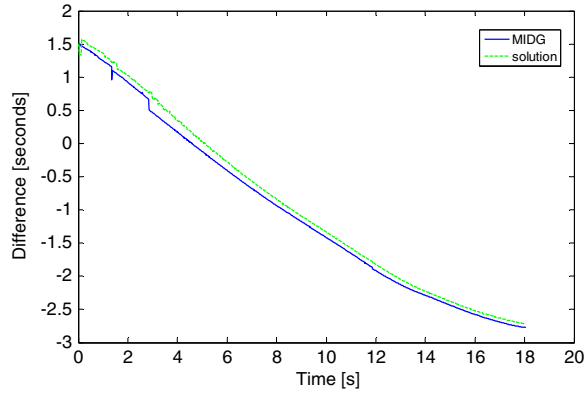

Fig. 37 Difference between the two vehicles in seconds for test 2 using EIF with velocity constraints

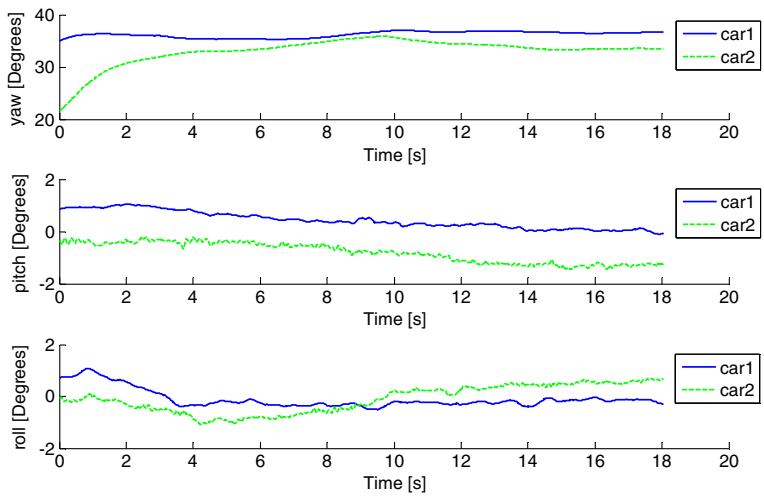

Fig. 38 Attitude estimates, two-vehicle dynamic test 2 using EIF with velocity constraints

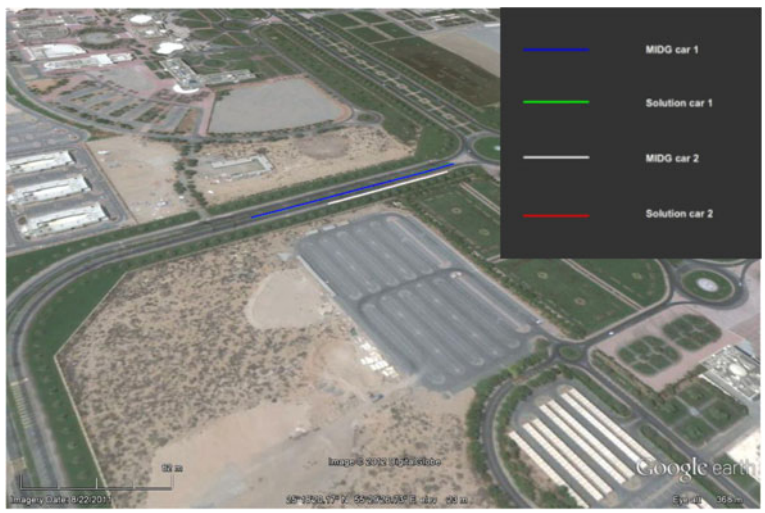

Fig. 39 Path estimates of the vehicles, two-vehicle dynamic test 3 using EIF with velocity constraints

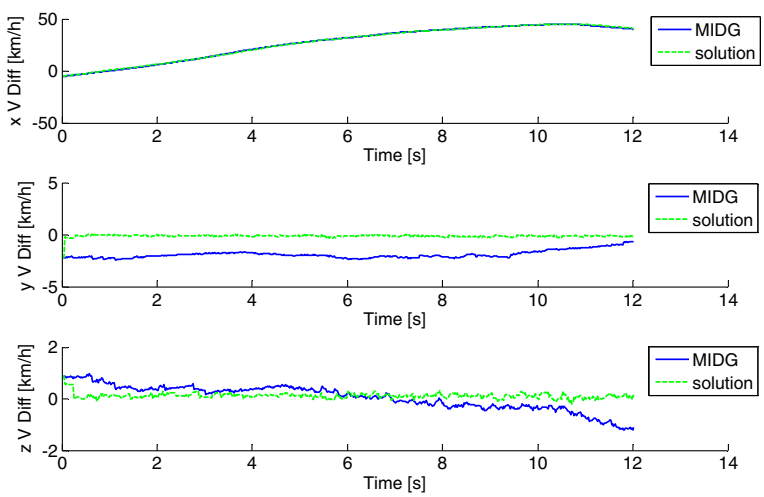

Fig. 40 Vehicle 2 velocity relative to vehicle 1 velocity in test 3 using EIF with velocity constraints

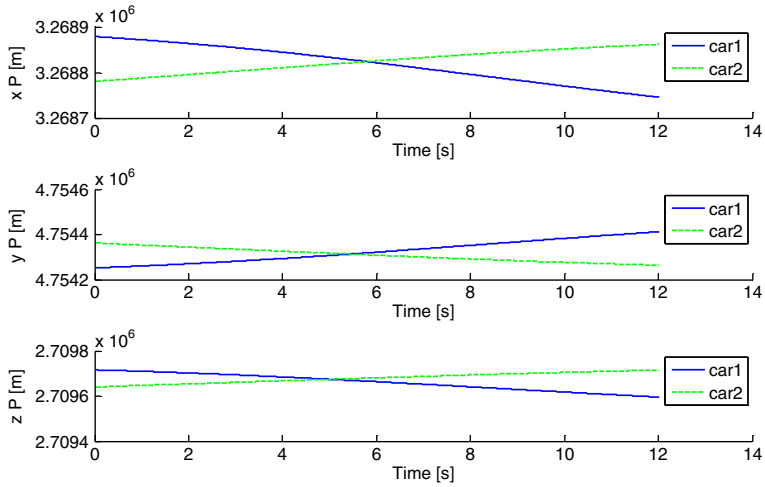

Fig. 41 Position estimates, two-vehicle dynamic test 3 using EIF with velocity constraints

it can be seen that vehicle 2 started to increase its speed in order to overtake vehicle 1 which was driving at around 50 km/h. Vehicle 2 then increased its velocity to reach about 70 km/h on the x axis. Figure 34 indicates that vehicle 2 had a higher forward velocity than vehicle 1. This is indicated by the negative relative velocity of vehicle 1 relative to vehicle 2 along the x axis of the body frame of vehicle 2.

Figure 35 shows the positions of both vehicles in the ECEF frame while Fig. 36 shows the position of vehicle 2 relative to vehicle 1 represented in the body frame of vehicle 2. As shown in Fig. 36, vehicle 2 crossed vehicle 1 at the fifth second of the test. This is also demonstrated in Fig. 37 which shows the relative time separation between the two vehicles as computed using Eq. 38. When vehicle 2 crossed to the left lane, the distance between the two vehicles on the y axis became close to 5 m. The negative values of the time difference between the two vehicles indicate that vehicle 2 crossed vehicle 1.

Figure 38 shows the yaw, pitch, and roll of the two vehicles in degrees. It can be noticed that when vehicle 2 was overtaking vehicle 1, the difference in the yaw angle was more than 10 degrees. This shows that vehicle 2 was overtaking vehicle 1 sharply. Afterwards, when vehicle 2 settled in the left lane, the change in yaw angle dropped close to zero.

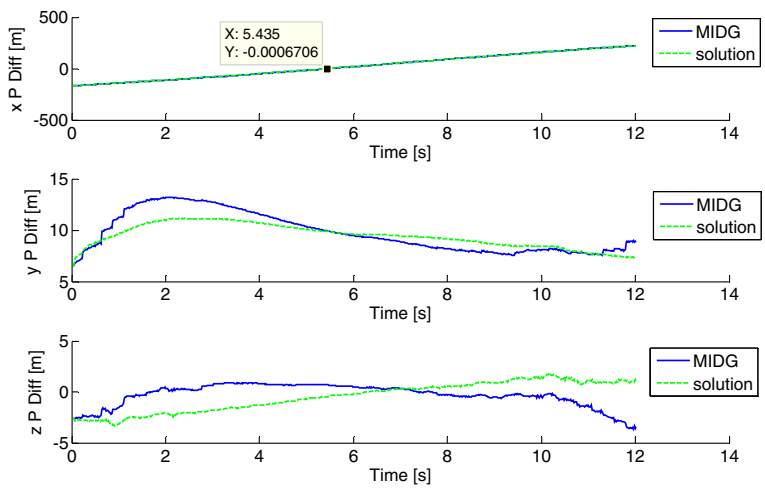

Fig. 42 Vehicle 2 position relative to vehicle 1 velocity in test 3 using EIF with velocity constraints

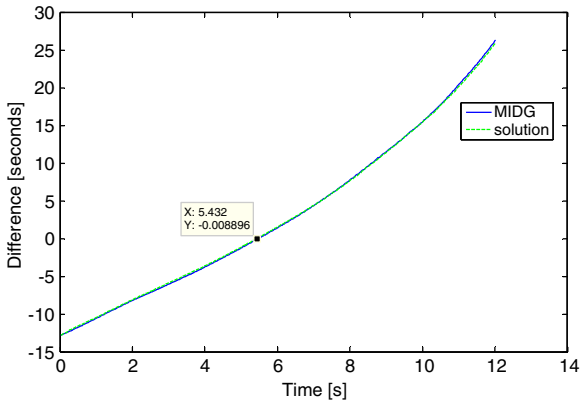

Fig. 43 Difference between the two vehicles in seconds for test 3 using EIF with velocity constraints

6.7 Two-Vehicle Dynamic Test 3 Using EIF with Velocity Constraints

Figures 39, 40, 41, 42, 43 and 44 show the results of a two-vehicle dynamic test where the EIF was used to fuse the measurements with the vehicles' dynamics. In this test, the two vehicles were heading towards each other, but on two different sides of the road. The test took 12 s. Figure 39 shows the path estimates of the two vehicles. Figure 40 shows the difference between the velocities of the two vehicles represented in the body frame of vehicle 2. The figure shows that the estimated relative velocity is in agreement with the relative velocity estimated by the MIDG.

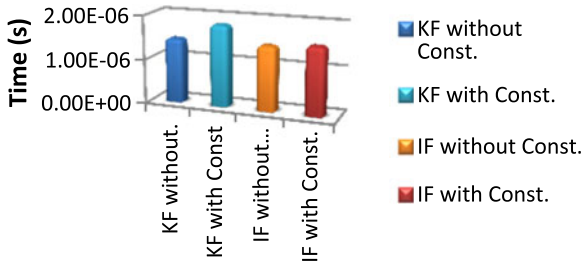

Fig. 45 Time taken for the two filters to be processed with and without velocity constraints by a 2.33 GHz dual-core processor

Figure 41 shows the positions of both vehicles in the ECEF frame while Fig. 42 shows the relative position between vehicle 1 and vehicle 2 represented in the body frame of vehicle 2. Figures 41 and 42 show that the two vehicles cross each other 5.4 s after the start of the test.

Figure 44 show that vehicle 1 was travelling southeast at an angle close to 123° and that vehicle 2 was travelling northwest at an angle close to 303° with an absolute difference of about 180° degrees between their heading angles. This demonstrates that the two vehicles were heading in opposite directions.

6.8 Processing Speed of the Two Filters

Figure 45 shows the time taken by a 2.33 GHz dual core processor to compute one cycle of the two

Fig. 44 Attitude estimates, two-vehicle dynamic test 3 using EIF with velocity constraints

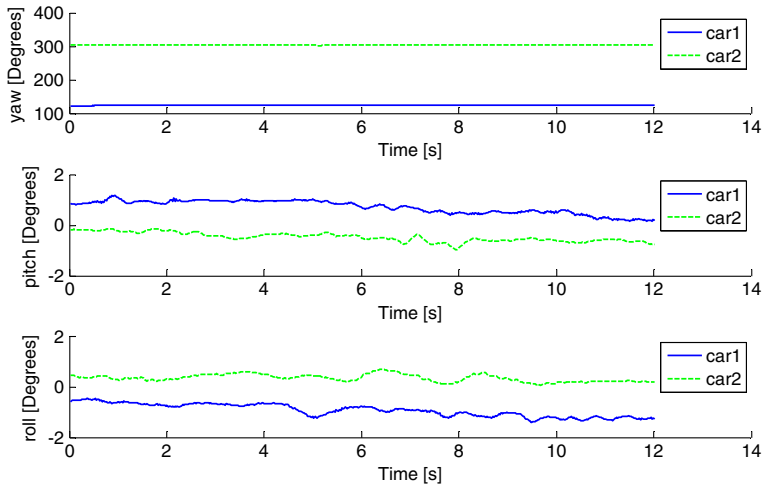

filters, once with velocity constraints fused and once with no velocity constraints fused.

From Fig. 45, it can be noticed that the EIF without constraints had the lowest processing time, and the EKF with velocity constraints had the highest processing time. With no constraints fused, the EIF was a little lower in terms of average computational time with about 1.4581×10^{-6} s for a single iteration, compared to the EKF without velocity constraints that took 1.4613×10^{-6} s for a single iteration. However, when the number of sensors increased and an encoder with velocity constraints on the y and z axes of the vehicle were fused with the measurements, the difference in the time taken became more considerable. With the constraints fused, the EKF took 1.84×10^{-6} s for one cycle on average, while the EIF took 1.535×10^{-6} s per cycle on average. This is about an 16.5 % reduction in computational time.

7 Conclusion

In this paper, a constrained, low-cost, GPS/IMU navigation algorithm is proposed. The filter utilizes the vehicle's axial body velocity measurements and nonholomonic constraints to improve the accuracy of the estimate. Both an extended Kalman filter and an extended information filter were used to estimate the vehicle's state. Various single-vehicle and two-vehicle experimental tests were conducted and the accuracy of the proposed methods was demonstrated. The results obtained were checked against a commercial standalone solution. Both the EKF and EIF showed consistent and high state-estimation accuracy. It was shown that the estimation error is substantially reduced when the velocity constraint measurement is used. This is especially seen in the body-frame y and z velocity estimates as they converge to zero, unlike results obtained without using the constraints which are shown to oscillate away from zero. The computational time of the EKF and the EIF implementations were analyzed. It was seen that more than a 16 % computational time reduction was achieved when using the EIF in comparison to the EKF. The proposed navigation algorithm can be utilized in the design of collision awareness/prevention systems.

References

1. Sahawneh, L.R., Al-Jarrah, M.A., Assaleh, K., Abdel-Hafez, M.F.: Real-time implementation of GPS aided low cost strapdown inertial navigation system. J. Intell. Robot. Syst. **61**(1–4), 527–544 (2011)
2. Sukkarieh, S.: Low cost, high integrity, aided inertial navigation systems for autonomous land vehicles. Ph.D. dissertation, Mechanical and Mechatronic Engineering, Australian Centre for Field Robotics, The University of Sydney, Sydney, Australia (2000)
3. Abdel-Hafez, M.F.: The autocovariance least squares technique for GPS measurement noise estimation. IEEE Trans. Veh. Technol. **59**(2), 574–588 (2010)
4. Noureldin, A., Karamat, T.B., Eberts, M.D., El-Shafie, A.: Performance enhancement of MEMS-based INS/GPS integration for low-cost navigation applications. IEEE Trans. Veh. Technol. **58**(3), 1077–1096 (2009)
5. Schelling, R.: A low-cost angular rate sensor for automotive applications in surface micromachining technology. In: 3rd Annual International Conference on Advanced Microsystems for Automotive Applications Proceedings (1999)
6. Belanović, P., Valerio, D., Paier, A., Zemen, T., Ricciato, F., Mecklenbräuker, C.F.: On wireless links for vehicle-to-infrastructure communications. IEEE Trans. Veh. Technol. **59**(1), 269–282 (2010)
7. Kinney, P.: ZigBee Technology: Wireless Control that Simply Works. Communications Design Conference (2003)
8. Biswas, S., Tatchikou, R., Dion, F.: Vehicle-to-vehicle wireless communication protocols for enhancing highway traffic safety. IEEE Commun. Magaz. **44**(1), 74–82 (2006)
9. Lahrech, A., Boucher, C., Noyer, J.-C.: Accurate vehicle positioning in urban areas. In: IMTC 2007—IEEE Instrumentation and Measurement Technology Conference, Warsaw, Poland, 1–3 May 2007
10. Che-Chung, L., Chi-Wei, L., Dau-Chen, H., Yung-Hsin, C.: Design a support vector machine-based intelligent system for vehicle driving safety warning. In: 11th International IEEE Conference on Intelligent Transportation Systems, pp. 938–943, 12–15 Oct 2008
11. Hightower, D.: Wireless technology advances crash avoidance. Microwaves & RF, pp. 22 (2010)
12. Santa, J., Toledo-Moreo, R., Zamora-Izquierdo, M.A., Ubeda, B., Gomez-Skarmeta, A.F.: An analysis of communication and navigation issues in collision avoidance support systems. Transp. Res. Part C. Emerg. Technol. **18**(3), 351–366 (2010)
13. Bonnabel, S., Salaün, E.: Design and prototyping of a low-cost vehicle localization system with guaranteed convergence properties. Control. Eng. Pract. **19**, 591–601 (2011)
14. Brandt, A., Gardner, J.F.: Constrained navigation algorithms for strapdown inertial navigation systems with reduced set of sensors. In: Proceedings of the American Control Conference (1998)

15. Dissanayake, G., Sukkarieh, S.: The aiding of a low-cost strapdown inertial measurement unit using vehicle model constraints for land vehicle applications. IEEE Trans. Robot. Autom. **17**(5), 731–747 (2001)
16. Noureldin, A., El-Shafie, A., Bayoumi, M.: GPS/INS integration utilizing dynamic neural networks for vehicular navigation. Inform. Fusion **12**, 48–57 (2011)
17. Kong, X.: INS algorithm using quaternion model for low cost IMU. Robot. Auton. Syst. **46**, 221–246 (2004)
18. Julier, S.J., Uhlmann, J.K., Durrant-Whyte, H.F.: A new approach for filtering nonlinear systems. In: Proceedings of the 1995 American Control Conference, pp. 1628–1632. Seattle, WA (1995)
19. Omni Instruments http://www.omniinstruments.co.uk/gyro/MIDGII.htm (2013). Accessed 14 July 2013